Power Factor in Control Lyapunov Functions for Electro-hydraulic Tracking Problem under the Influence of Friction

Honorine Angue Mintsa [1,*], Géremino Ella Eny [2], Rolland Michel Assoumou Nzué[1], and Nzamba Senouveau [3]

[1] Department of Mechanical Engineering, Polytechnical School of Masuku, University of Sciences and Technologies of Masuku, Franceville, Gabon
[2] Department of Physics, Faculty of Sciences, University of Sciences and Technologies of Masuku, Franceville, Gabon
[3] Department of Electrical Engineering, Polytechnical School of Masuku, University of Sciences and Technologies of Masuku, Franceville, Gabon
Email: honorine.angue@univ-masuku.org (H.A.M.); ellaenyg@yahoo.fr (G.E.E.); rollandassoumou82@yahoo.fr (R.M.A.N.); senouveau@yahoo.fr (N.S.)
*Corresponding author

***Abstract*—Control Lyapunov Function (CLF) is a powerful tool for synthesizing nonlinear control laws. Several control laws may be deduced from the same CLF. In the Electro-hydraulic Servo Systems (EHSS) literature, two types of CLF are distinguished, especially for tracking control problems. The first type is a sum of a quadratic function of the errors while the second type is the quadratic function of the weighted sum of the errors. In this paper, we extend the second type of CLF by adding a power factor to appreciate its influence on closed-loop performances. Thus, we obtain three CLFs instead of the classic quadratic function by varying the power factors 2, 4 and 6. The three deducing control laws are compared under the presence of Coulomb friction. The study is carried out both for an angular velocity tracking control and an angular position tracking control. The numerical results show that the control laws using the CLFs of orders 2 and 4 have the best performances. Moreover, the closed-loop systems based on both controllers exhibit the best robust results under friction disturbance.**

***Keywords*—Control Lyapunov Function (CLF), Sontag formula, Electro-hydraulic Servo Systems (EHSS), Lyapunov redesign control, friction, weighted tracking errors sum**

I. Introduction

Engineering applications require Electro-hydraulic Servo Systems (EHSS) to manipulate large mechanical loads with a fast, robust and accurate response. Common examples include aerospace actuation [1], automobile active suspension actuation [2], machine tool actuation [3], lift system actuation [4], and drilling process actuation [5]. PID controllers are widely used to control those machines because of their simplicity, flexibility and well-established design [6]. Xiang *et al.* [7] apply PID regulators based on a hydraulic excavator model and highlight the complexity of the control adjustment due to the incomplete information about the dynamics of the system and its interactions with the earth's environment. Thus, the performances obtained by this linear control theory are limited around an operating point [8]. The EHSS has nonlinear dynamics with hydraulic parameter uncertainties [9]. Moreover, frictions and external disturbances lead the overall system away from the operating point [7].

Among the existing nonlinear control laws in the literature, the Lyapunov Redesign (LR) approach offers powerful solutions. LR is based on the design of the Control Lyapunov Function (CLF). A CLF is a positive definite function whose time derivative is made negative definite by choosing an appropriate control law. This approach allows the design of an original control law while ensuring asymptotic stability [10]. Unlike the feedback linearization approach which cancels all system nonlinearities, the LR approach selects the nonlinearity to be cancelled. Thus, robust performance is achieved using this technique. In the EHSS literature, backstepping control [11], sliding mode control [12] and control based on Sontag's formula [13] are control theories based on the Lyapunov Redesign approach and give good results. The main obstacle to the LR approach is the determination of the CLF. First, this positive definite function must include all the system state variables. For EHSS, the system variable states may reach the number five. Second, the input signal must appear after a single time derivative of the CLF. Finally, an analytic control law is found to make the time derivative of the CLF negative definite. One can note that the LR has two flexible steps: the choice of the CLF and the choice of the analytic structure of the control law.

In 1982, Lyapunov functions appeared in literature to provide proof of the asymptotic stability of nonlinear

Manuscript received May 18, 2023; revised August 14, 2023; accepted September 13, 2023; published January 29, 2024.

systems [14]. Initially, LFs are used in aerospace applications to control the satellite altitude or to describe orbital motion [15] using the total energy. Due to the presence of friction, the total energy decreases over time. Indeed, the total energy is an excellent Lyapunov candidate function for these mechanical systems because its time derivative is a negative definite function. However, for most systems, not all the state variables are included in this energy function. Moreover, for tracking control systems, the tracking error and its time derivatives are more relevant than the system state variables themselves [16–18]. The disadvantage of this approach is the difficulty of demonstrating that the time derivative of the selected LF is negative definite. In 1983, Artstein [19] circumvented the problem by introducing the Control Lyapunov Function (CLF) which is a LF that includes the input control signal, which has to be designed. Hence, the control strategy consists of finding control algorithms that make the time derivative of the CLF a negative definite function. Based on Artstein's results, Sontag [20] builds an elaborate version of CLF using the Lie derivatives of the system and finds an analytic control solution based on the Riccati equation.

To our knowledge, only two types of CLF are used in the EHSS literature. The first type of CLF is obtained by a recursive method or backstepping. This approach consists of dismantling the EHSS into several first-order subsystems. A piecewise CLF is constructed for each subsystem. Kaddissi *et al.* [11] back step four subsystems to derive the final CLF and deduce the control law for EHSS. However, this strategy is very painful because the recursive steps increase with the system order leading the closed-loop system to an explosion of complexity. The second type of CLF comes from the Artstein / Sontag analytical expression [20]. Because the input signal should appear in the first time derivative of the CLF, Mintsa *et al.* [13] choose the weighted sum of the tracking error as CLF. As is explained in [21] and in sliding mode theory [22], the time derivative of the weighted sum of the tracking error makes the input signal appear after one time derivation [24]. Most of the CLFs in the literature are quadratic functions to provide positive definite functions. Quadratic functions are well established to study system stability [23]. Recent works show that non quadratic Lyapunov functions lead to higher robustness in the system performances [24].

In this paper, we address the analysis of different non-quadratic CLFs architectures derived from our previous work [13]. In addition to the velocity servo control, we extend the study to the angular position servo control. The objective is to compare the closed-loop performances using the same analytic control solution with different opportunities of CLF. We vary the conventional power factor of 2 in the CLF with a power factor of 4 and 6.

The rest of the paper is organized as follows: Section II describes the EHSS under study and its mathematical model. Section III shows the development of the control laws based on the three different CLFs. Section IV presents the numerical simulation results and the discussion. Finally, the conclusion is drawn in Section V.

II. System Modeling

The electrohydraulic servo system under study is shown in Fig. 1. It consists of a hydraulic bidirectional motor that drives a rotational mechanical load. The hydraulic power pack includes the oil tank, the pump, the relief valve and the accumulator. Its objective is to supply hydraulic oil at a constant pressure in the servo valve entry. The electrohydraulic servo valve ensures the interface between the operative part and the control part. The input signal u(t) is the output of the feedback control law. In this study, the outputs of interest are the angular velocity $\dot{\theta}(t)$ of the motor sensed by the feedback transducer and the angular position which is the time integration of the velocity. The desired angular velocity and the desired angular position are obtained via the reference signal.

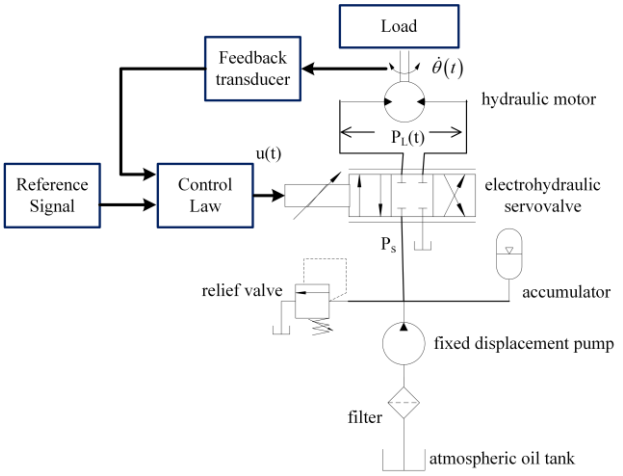

Fig. 1. Electro-hydraulic servo system.

The following assumptions are considered in this section:

- The saturation and the hysteresis in the electrohydraulic servo valve are neglected.
- The external disturbances are not taken into account.
- The servo valve dynamics are approximated to a first-order system.

Besides the time integration of the angular velocity, the dynamics of the EHSS are dismantled into three subsystems as shown in the state-space equation Eq. (1). The first subsystem describes the equation of motion of the rotational load. The second subsystem shows the equation of continuity through the hydraulic motor lines. The second subsystem is the servo valve dynamics.

$$\begin{aligned}
\dot{x}_1(t) &= x_2(t) \\
\dot{x}_2(t) &= \frac{d_m}{J}x_3(t) - \frac{B_m}{J}x_2(t) - \frac{T_f(t)}{J} \\
\dot{x}_3(t) &= \frac{4\beta c_d}{V_m}\left(x_4(t)\frac{c_d}{\sqrt{\rho}}\sqrt{P_s - sign\left(x_4(t)\right)x_3(t)} - d_m x_2(t) - c_{sm}x_3(t) \right) \\
\dot{x}_4(t) &= \frac{K}{\tau}u(t) - \frac{1}{\tau}x_4(t)
\end{aligned} \tag{1}$$

where

$x_1(t)$ is the angular position $\theta(t)$

$x_2(t)$ is the angular velocity $\dot{\theta}(t)$

$x_3(t)$ is the motor pressure difference $P_L(t)$ due to the load

$x_4(t)$ is the servo valve opening area due to the input signal

$u(t)$ is the control current input

$T_f(t)$ is the coulomb friction disturbance

J is the hydraulic motor total inertia

d_m is the volumetric displacement of the motor

β is the fluid bulk modulus

V_m is the total oil volume of the hydraulic motor

c_d is the servo valve discharge coefficient

ρ is the fluid mass density

c_{sm} is the leakage coefficient of the hydraulic motor

P_s is the supply pressure at the inlet of the servo valve

K is the servo valve amplifier gain

τ is the servo valve time constant

To satisfy the Lipshitz conditions in the mathematical model [29], we replace the non-differentiable sign function with the continuously differentiable sigmoid function described in Eq. (2) and detailed in [25]:

$$sign(x(t)) \simeq \frac{x(t)}{\sqrt{x^2(t)+\delta_x}} = sigm(x(t)) \;;\; \delta_x > 0 \quad (2)$$

where we assume:

$$\lim_{\delta_x \to \infty} \frac{dsigm(x(t))}{dt} = 0 \quad (3)$$

The sigmoid parameter δ is adjusted based on the x domain to have the S-shaped as shown in Fig. 2. When the values of x are close to 10^{-8}, the parameter of the sigmoid function is adjusted to 10^{-18}. When the values of x are close to 1, the parameter of the sigmoid function is adjusted to 10^{-3}.

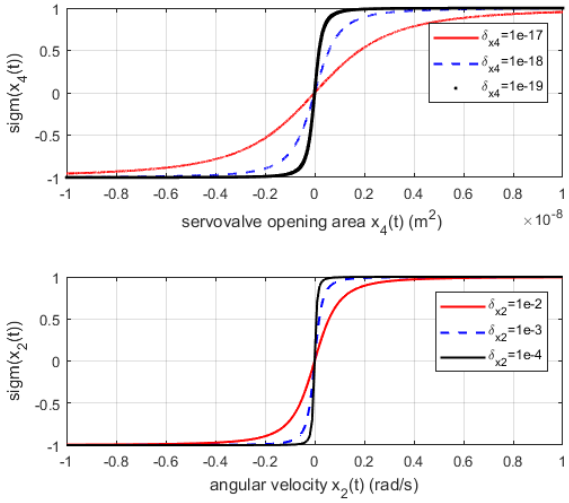

Fig. 2. Parameters effect on sigmoid function.

III. Controllers Design Based on CLF

In this section, the design of the three controllers based on three CLFs is presented. We use the same control law established in our previous work [13]. It consists of a Lyapunov redesign control law based on the Sontag formula [20]. The objective is to vary the power factor in our previous CLF to obtain three CLF opportunities. In this paper, only the outline of the controller design is followed and shown in Fig. 3. For more details, readers can refer to our previous work [13, 26].

The design is focused on the development of the angular velocity tracking controller of the EHSS. In subsection B, we extend the design to develop the angular position tracking controllers.

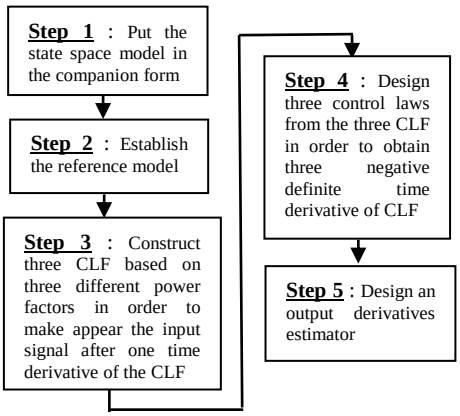

Fig. 3. Design of three Lyapunov redesign controllers from three CLF.

The first step consists of writing the EHSS model of Eq. (1) in the companion form (Eq. (4))[13, 26]:

$$\dddot{y}(t) = \sum_{i=1}^{6} a_i f_i(x,t) + g(x,t)u(t) \quad (4)$$

where the output equation of the Eq. (1) is $y(t) = \dot{\theta}(t)$

$$g(x,t) = \frac{4\beta D_m c_d K}{J\tau V_m \sqrt{\rho}} \sqrt{P_s - x_3(t) sigm(x_4(t))}$$

$$f_1(x,t) = x_2(t)$$

$$f_2(x,t) = x_3(t)$$

$$f_3(x,t) = x_4(t)\sqrt{P_s - x_3(t) sigm(x_4(t))}$$

$$f_4(x,t) = x_4(t)x_4(t) sigm(x_4(t))$$

$$f_5(x,t) = \frac{x_2(t)x_4(t) sigm(x_4(t))}{\sqrt{P_s - x_3(t) sigm(x_4(t))}}$$

$$f_6(x,t) = \frac{x_3(t)x_4(t) sigm(x_4(t))}{\sqrt{P_s - x_3(t) sigm(x_4(t))}}$$

$$a_1 = \frac{8\beta B d_m^2 J V_m - B^3 V_m^2 + 16\beta^2 d_m^2 c_{sm} J^2}{J^3 V_m^2}$$

$$a_2=\frac{B^2V_m^2d_m-4\beta d_m^3JV_m+16\beta^2d_mc_{sm}^2J^2+4\beta Bd_mV_mc_{sm}J}{J^3V_m^2}$$

$$a_3=-\frac{\tau\left(16\beta^2c_dd_mc_{sm}J+4\beta c_dBd_mV_m\right)+4\beta d_mc_dJV_m}{\tau J^2V_m^2\sqrt{\rho}}$$

$$a_4=-\frac{8\beta^2d_mc_d^2}{JV_m^2\rho}$$

$$a_5=\frac{8\beta^2d_mc_dc_{sm}}{JV_m^2\sqrt{\rho}}$$

$$a_6=\frac{8\beta^2d_mc_dc_{sm}}{JV_m^2\sqrt{\rho}}$$

The second step is to describe the desired trajectory of the state by considering the three-order reference model shown in Eq. (5).

$$\dddot{y}_{des}(t)+\alpha_2\ddot{y}_{des}(t)+\alpha_1\dot{y}_{des}(t)+\alpha_0y_{des}(t)=r(t) \quad (5)$$

where $y_{des}(t)=\dot{\theta}_{des}(t)$ and $r(t)$ are the desired output and the input of the reference model respectively. The coefficient α_i are distributed in the Butterworth pattern.

The third step is to choose a CLF that includes all the system variable states. Now, we propose a CLF different from our previous work by varying the power factor 2.

$$V_n(x,t)=\frac{s^n(x,t)}{n} \qquad n=2,4\ and\ 6 \quad (6)$$

where $s(x,t)=\ddot{e}(t)+\lambda_1\dot{e}(t)+\lambda_0e(t)$ is the combined error or the weighted sum of the velocity error $e(t)=y(t)-y_{des}(t)$. The coefficients λ_i are distributed according to the Butterworth model. In the sliding mode control design, the combined error is well-known as the sliding surface [18]. In Eq. (6), the power factor n ensures the positive definition of the CLF only if n is an even number. For the remainder of this study, we use three power factors as shown in Eq. (7)–Eq. (9) to deduce three CLFs of order 2, 4 and 6.

$$V_2(x,t)=\frac{s^2(x,t)}{2} \quad (7)$$

$$V_4(x,t)=\frac{s^4(x,t)}{4} \quad (8)$$

$$V_6(x,t)=\frac{s^6(x,t)}{6} \quad (9)$$

The fourth step is to calculate the time derivative of the three CLFs to bring up the input control signal.

$$\dot{V}_2(x,t)=s(x,t)\left(\sum_{i=1}^{6}a_if_i(x,t)+g(x,t)u(t)-\dddot{y}_{des}+\lambda_1\ddot{e}(t)+\lambda_0\dot{e}(t)\right) \quad (10)$$

$$\dot{V}_4(x,t)=s^3(x,t)\left(\sum_{i=1}^{6}a_if_i(x,t)+g(x,t)u(t)-\dddot{y}_{des}+\lambda_1\ddot{e}(t)+\lambda_0\dot{e}(t)\right) \quad (11)$$

$$\dot{V}_6(x,t)=s^5(x,t)\left(\sum_{i=1}^{6}a_if_i(x,t)+g(x,t)u(t)-\dddot{y}_{des}+\lambda_1\ddot{e}(t)+\lambda_0\dot{e}(t)\right) \quad (12)$$

Next, we extend the Sontag's formula according to [20] and [13] to obtain the three following control laws:

$$u_2(t)=\begin{cases}-\dfrac{\left(s(x,t)\left(\sum_{i=1}^{6}a_if_i(x,t)-\dddot{y}_{des}(t)+\lambda_1\ddot{e}(t)+\lambda_0\dot{e}(t)\right)\right.\\ \left.+\sqrt{\left(s(x,t)\sum_{i=1}^{6}a_if_i(x,t)\right)^2+\left(s(x,t)g(x,t)\right)^4}\right)}{s(x,t)g(x,t)}, & s(x,t)\neq0\\ 0, & s(x,t)=0\end{cases} \quad (13)$$

$$u_4(t)=\begin{cases}-\dfrac{\left(s^3(x,t)\left(\sum_{i=1}^{6}a_if_i(x,t)-\dddot{y}_{des}(t)+\lambda_1\ddot{e}(t)+\lambda_0\dot{e}(t)\right)\right.\\ \left.+\sqrt{\left(s^3(x,t)\sum_{i=1}^{6}a_if_i(x,t)\right)^2+\left(s^3(x,t)g(x,t)\right)^4}\right)}{s^3(x,t)g(x,t)}, & s(x,t)\neq0\\ 0, & s(x,t)=0\end{cases} \quad (14)$$

$$u_6(t)=\begin{cases}-\dfrac{\left(s^5(x,t)\left(\sum_{i=1}^{6}a_if_i(x,t)-\dddot{y}_{des}(t)+\lambda_1\ddot{e}(t)+\lambda_0\dot{e}(t)\right)\right.\\ \left.+\sqrt{\left(s^5(x,t)\sum_{i=1}^{6}a_if_i(x,t)\right)^2+\left(s^5(x,t)g(x,t)\right)^4}\right)}{s^5(x,t)g(x,t)}, & s(x,t)\neq0\\ 0, & s(x,t)=0\end{cases} \quad (15)$$

We recall that the function $g(x,t)$ is always strictly positive because the pressure difference across the motor line never exceeds $2P_s/3$ for the servo valve requirements [9]. Finally, with these control laws, the time derivative of the three CLFs become:

$$\dot{V}_2(x,t)=-\sqrt{\left(s(x,t)\sum_{i=1}^{6}a_if_i(x,t)\right)^2+\left(s(x,t)g(x,t)\right)^4} \quad (16)$$

$$\dot{V}_4(x,t)=-\sqrt{\left(s^3(x,t)\sum_{i=1}^{6}a_if_i(x,t)\right)^2+\left(s^3(x,t)g(x,t)\right)^4} \quad (17)$$

$$\dot{V}_6(x,t)=-\sqrt{\left(s^5(x,t)\sum_{i=1}^{6}a_if_i(x,t)\right)^2+\left(s^5(x,t)g(x,t)\right)^4} \quad (18)$$

The three CLFs are negative definite because $V_{2,4,6}(x,t)=0$ if $s(x,t)=0$. Thus, the asymptotic stability of the three closed-loop systems is ensured. Fig. 4 shows the implementation of the controlled closed-loop system in the Matlab / Simulink environment.

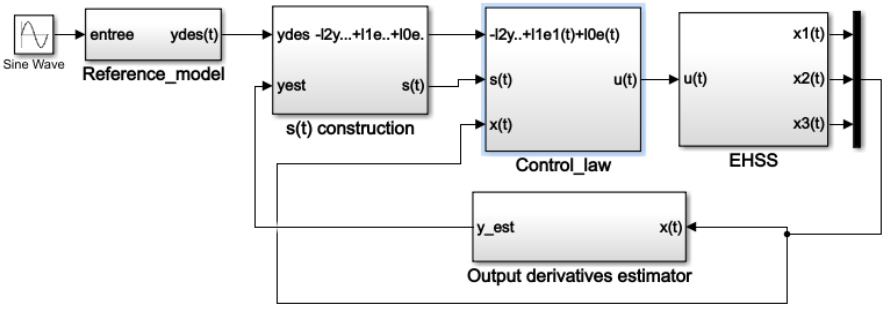

Fig. 4. The block diagram of the EHSS closed loop controlled EHSS.

The output derivatives are calculated using a model of the form:

$$\ddot{y}_{est}(t)+\beta_1\dot{y}_{est}(t)+\beta_0 y_{est}(t)=y_{act}(t) \qquad (19)$$

where $y_{act}(t)$ and $y_{est}(t)$ are the measured actual output and the estimated output. The coefficients β_i are distributed according to the Butterworth pattern.

A. *Extension of the Design for the Angular Position Tracking Control*

In this subsection, the main lines of the previous development are taken up to design the three control laws for tracking the angular position. The system output becomes the angular position of the load. The angular position $\theta(t)$ is the time integration of the angular velocity $\dot{\theta}(t)$. Hence, the companion form becomes a four-order system.

$$\dddot{y}_p(t)=\sum_{i=1}^{6}a_i f_i(x,t)+g(x,t)u(t) \qquad (20)$$

where the output equation of the Eq. (1) becomes $y_p(t)=\theta(t)$.

A four-order reference model Eq. (21) replaces the three-order reference model of Eq. (5).

$$\dddot{y}_{p\_des}(t)+\alpha_{3p}\ddot{y}_{p\_des}(t)+\alpha_{2p}\ddot{y}_{p\_des}(t)+\alpha_{1p}\dot{y}_{p\_des}(t)+\alpha_{0p}y_{p\_des}(t)=r(t) \qquad (21)$$

where $y_{p\_des}(t)=\theta_{des}(t)$ is the desired output for the angular position control. The coefficient α_{ip} are distributed in the Butterworth pattern. For the angular position, the combined error $s_p(x,t)$ is

$$s_p(x,t)=\dddot{e}_p(t)+\lambda_{2p}\ddot{e}_p(t)+\lambda_{1p}\dot{e}_p(t)+\lambda_{0p}e_p(t) \qquad (22)$$

where the position tracking error is $e_p(t)=y_p(t)-y_{p\_des}(t)$. The coefficients λ_{ip} are distributed according to the Butterworth model. The three angular position control laws based on the three power factors are

$$u_{p\_n\ n=2,4,6}(t)=\begin{cases}-\dfrac{\left(s_p^{n-1}(x,t)\left(\sum_{i=1}^{6}a_i f_i(x,t)-\dddot{y}_{des}(t)+\lambda_{2p}\ddot{e}(t)+\lambda_{1p}\dot{e}(t)+\lambda_{0p}\dot{e}(t)\right)\right.}{\left.+\sqrt{\left(s_p(x,t)\sum_{i=1}^{6}a_i f_i(x,t)\right)^2+\left(s_p(x,t)g(x,t)\right)^4}\right)} & ,s_p(x,t)\neq 0 \\ s_p^{n-1}(x,t)g(x,t) & \\ 0 & ,s_p(x,t)=0\end{cases} \qquad (23)$$

Finally, for the angular position controller, the output derivatives estimator becomes

$$\dddot{y}_{p\_est}(t)+\beta_{2p}\ddot{y}_{p\_est}(t)+\beta_{1p}\dot{y}_{p\_est}(t)+\beta_{0p}y_{p\_est}(t)=y_{p\_act}(t) \qquad (24)$$

where $y_{p\_act}(t)$ and $y_{p\_est}(t)$ are the measured actual output and the estimated output. The coefficients β_{ip} are distributed according to the Butterworth pattern.

IV. Results and Discussion

In this section, the performances of the three controllers are presented, analysed and compared. The simulation is executed under the Matlab/ Simulink environment for 20 s with a sampling time of 10 ms. The input signal used for this study is a sine wave with an amplitude of 1 rad/s and a frequency of 2 rad/s. The numerical data used for the simulation are tabulated in Table I.

TABLE I. The Numerical Data Used for the Simulation

Symbol	Description	Value and units
	EHSS	
δ_{x_1}	Sigmoid function constant for $x_1(t)$	0.001
τ	Servo valve time constant	0.01 s
δ_{x_3}	Sigmoid function constant for $x_3(t)$	10^{-18}
K	Servo valve amplifier gain	8.10^{-7} m²/mA
V_m	Total oil volume of the motor	3×10^{-4} m³
β	Fluid bulk modulus	8×10^{8} Pa
c_d	Flow discharge coefficient	0.61
P_s	Supply pressure	9×10^{6} Pa
c_{sm}	Leakage coefficient	9×10^{-13} m⁵/ (N.s)
d_m	Volumetric displacement of the motor	3×10^{-6}m³/rad
ρ	Fluid mass density	900 Kg/m³
J	Total inertia of the motor and the load	0.05 N.m.s²

B	Viscous damping coefficient	0.2 N.m.s
T_f	Friction term	1.8 *Nm*
Reference Model for the angular velocity controller		
α_2	Coefficient for the reference model	$2(2\pi\times 20)$
α_1	Coefficient of the reference model	$2(2\pi\times 20)^2$
α_0	Coefficient of the reference model	$(2\pi\times 20)^3$
Reference Model for the angular position controller		
α_{0p}	Coefficient for the reference model	$(2\pi\times 20)^4$
α_{1p}	Coefficient for the reference model	$2.61(2\pi\times 20)^3$
α_{2p}	Coefficient for the reference model	$3.41(2\pi\times 20)^2$
α_{3p}	Coefficient for the reference model	$2.61(2\pi\times 20)$
Proposed angular velocity Controller		
f_r	Cutoff frequency for the combined error	100 *Hz*
λ_1	Coefficient for the combined error	$\sqrt{2}(2\pi\times f_r)$
λ_0	Coefficient for the combined error	$(2\pi\times f_r)^2$
δ_c	Sigmoid function constant for the controller	10^{-3}
Proposed angular position Controller		
λ_{2p}	Coefficient for the combined error	$2(2\pi\times 60)$
λ_{1p}	Coefficient for the combined error	$2(2\pi\times 60)^2$
λ_{0p}	Coefficient for the combined error	$(2\pi\times 60)^3$
Output derivatives Estimator for the angular velocity controller		
β_1	Coefficient of the estimator model	$\sqrt{2}(2\pi\times 1000)$
β_0	Coefficient of the estimator model	$(2\pi\times 1000)^2$
Output derivatives Estimator for the angular position controller		
β_{2p}	Coefficient for the estimator model	$2(2\pi\times 1000)$
β_{1p}	Coefficient for the estimator model	$2(2\pi\times 1000)^2$
β_{0p}	Coefficient for the estimator model	$(2\pi\times 1000)^3$

In order to evaluate the robustness of the three controllers, we simulate a Coulomb friction disturbance between 8 and 10 s in the hydraulic motor. As shown in Fig. 5, the amplitude of the friction reaches 10% of the maximal mechanical torque applied to the load.

$$T_f(t)=1.8sgm(x_2(t)) \quad (25)$$

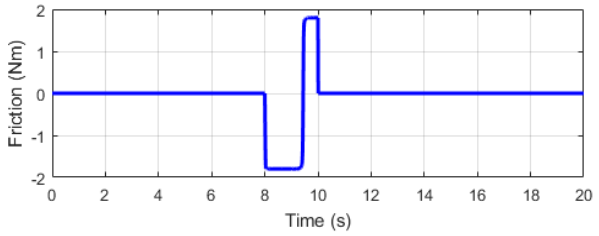

Fig. 5. Simulation of Coulomb friction disturbance.

A. *Angular Velocity Controllers Results*

Figs. 6 and 7 show the closed-loop responses obtained with the three controllers. We wanted to execute the closed-loop system with the same combined error cutoff frequency of our previous work which is 100 Hz [13]. Recall that the combined error is a Butterworth polynomial filter. The two first responses obtained with $u_2(t)$ and $u_4(t)$ show good results. Between 8s and 10s, when the Coulomb friction operates, the closed-loop responses obtained with these two controllers show excellent robustness with slight overshoots visible in Fig. 7. When using the controller $u_6(t)$, the tracking performances are good up to 8 s. After 8 s, high frequency sustained oscillations with large amplitude are observed until the end of the simulation. Between 8 s and 10 s, the amplitude of the sustained oscillations is about 15 rad/s while the amplitude reaches 18 rad/s after 10 s. The closed loop based on the CLF of power factor 6 shows less robustness. The power factor of 5 in the control signal $u_6(t)$ provides a large deviation in the tracking error leading the closed-loop systems to instability when disturbances occur. Power factors 2 and 4 amplify the tracking error deviation without moving it away from the region of asymptotic stability.

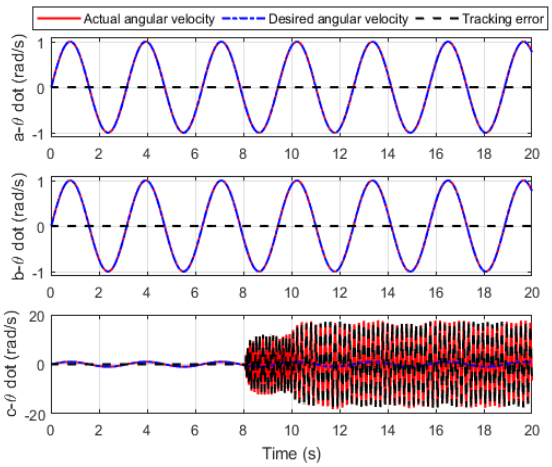

Fig. 6. System response when using (a) the control law $u_2(t)$; (b) the control law $u_4(t)$; (c) the control law $u_6(t)$ for $f_r=100\,Hz$.

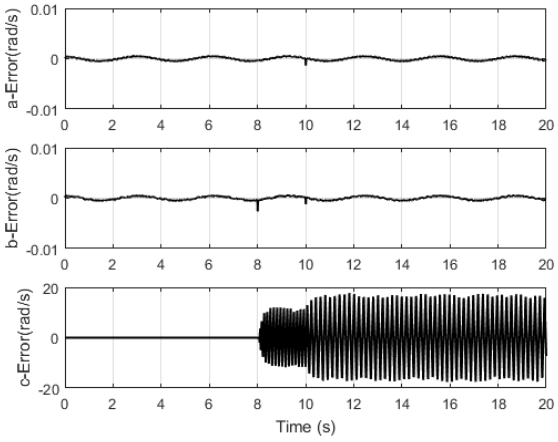

Fig. 7. Tracking error when using (a) the control law $u_2(t)$; (b) the control law $u_4(t)$; (c) the control law $u_6(t)$ for $f_r=100\,Hz$.

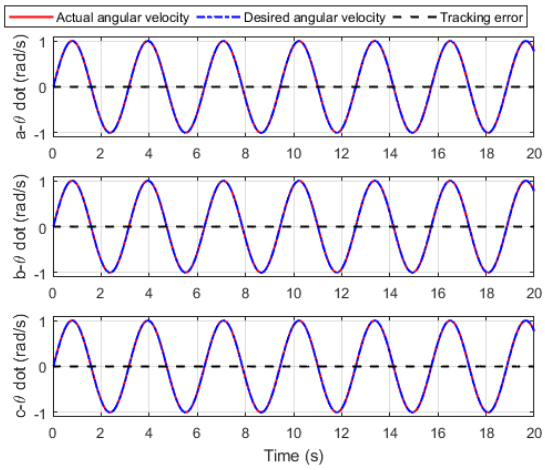

Fig. 8. System response when using (a) the control law $u_2(t)$; (b) the control law $u_4(t)$; (c) the control law $u_6(t)$ for $f_r = 60\,Hz$.

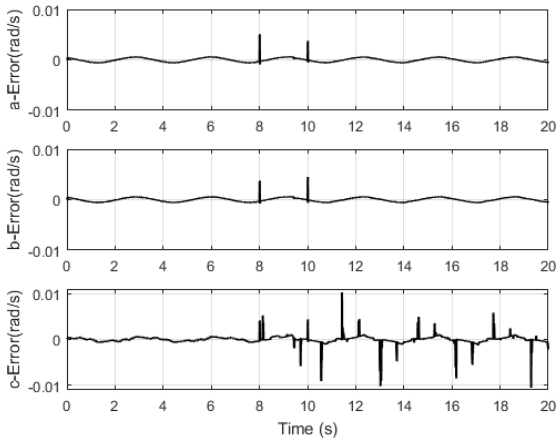

Fig. 9. Tracking error when using (a) the control law $u_2(t)$; (b) the control law $u_4(t)$; (c) the control law $u_6(t)$ for $f_r = 60\,Hz$.

To reduce the high-frequency sustained oscillations in the closed-loop response seen earlier with the controller $u_6(t)$, we reduce the cutoff frequency to 60 Hz. Figs. 8 and 9 illustrate the closed-loop responses for the three controllers with a combined error cutoff frequency of 60 Hz. We see that reducing the cutoff frequency increases the robustness of the controller by suppressing high-frequency sustained oscillations in the tracking error. Again, CLF based controllers with powers factor 2 and 4 perform well. Their closed-loop responses correctly follow the desired angular velocity with a negligible error when there is no friction (see Fig. 9 (a), (b)). Between 8 and 10 seconds, when friction occurs, both closed-loop responses show almost the same slight overshoots at 8 s and 10 s. However, the third closed-loop EHSS response shown in Fig. 9(c), the one based on the CLF with a power factor of 6, gives the least satisfactory results. Small chattering is visible after 8 s.

Fig. 10 shows the control signal obtained during the simulation. It is noted that the three controllers develop large effort with amplitude reaching 10^{10} A for the controller based on the CLF of power factor 2, 10^{13} A for the controller based on the CLF of power factor 4 and 10^{18} A for the controller based on the CLF of power factor 6. Chattering is well-known in controlled systems using Lyapunov Redesign [27]. Severe chattering is unacceptable for the actuator input signal because it causes rapid system wear. However, there is a trade-off between the fluctuation in control input and the steady state error [28]. The controller parameters and the output derivatives estimator play a role in the closed-loop performances. Other settings of these different parameters are necessary to obtain an acceptable control signal. Strategies could also be grafted onto the controller to help it to reduce or eliminate chattering [29].

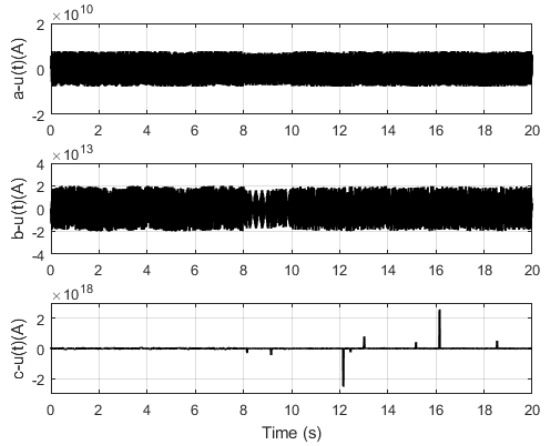

Fig. 10. Control signal when using (a) the control law $u_2(t)$, (b) the control law $u_4(t)$ and (c) the control law $u_6(t)$ for $f_r = 60\,Hz$.

B. Angular Position Controllers Results

In this subsection, we present the results obtained with the angular position controllers. Figs. 11 and 12 show the closed-loop responses with the cutoff frequency to 60 Hz. Good results are achieved with the three controllers. Again, the control law with the power factor 6 shows insufficiencies of robustness. Fig. 13 shows the control signal of the three controllers with the cutoff frequency of 60 Hz. We can see that significant chattering is present.

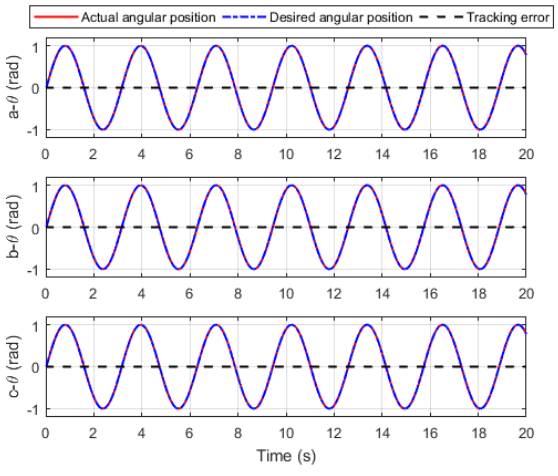

Fig. 11. System response when using (a) the control law $u_{p2}(t)$, (b) the control law $u_{p4}(t)$ and (c) the control law $u_{p6}(t)$ for $f_r = 60\,Hz$.

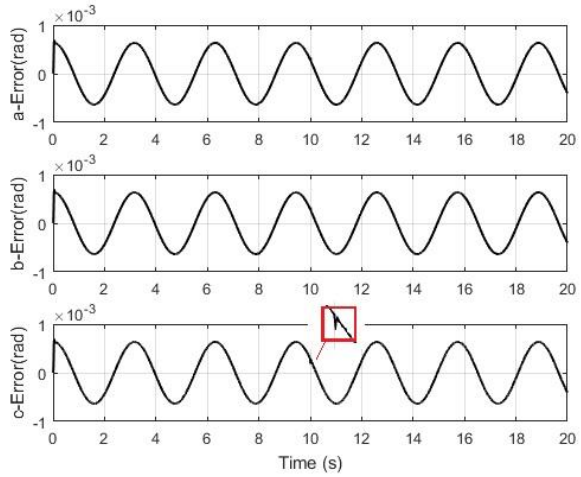

Fig. 12. Tracking error when using (a) the control law $u_{p2}(t)$, (b) the control law $u_{p4}(t)$, (c) the control law $u_{p6}(t)$ for $f_r = 60\,Hz$.

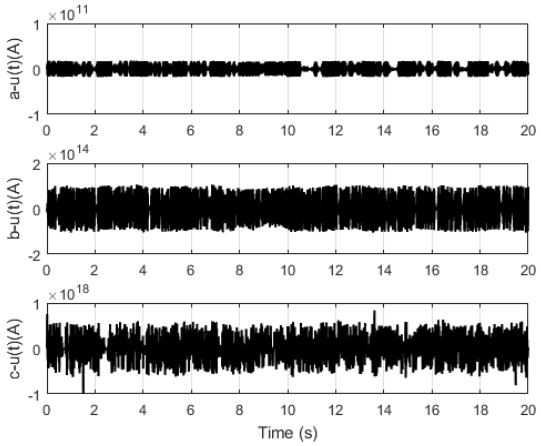

Fig. 13. Control signal when using (a) the control law $u_{p2}(t)$, (b) the control law $u_{p4}(t)$ and (c) the control law $u_{p6}(t)$ for $f_r = 60\,Hz$.

V. Conclusion

In this paper, we investigate the performances of a nonlinear Lyapunov redesign controller based on Sontag's formula from three different control Lyapunov functions. The study is carried out both for an angular velocity tracking control and an angular position tracking control. The three control Lyapunov functions are a weighted sum of the tracking error and its time derivatives to which we apply a power factor of 2, 4 and 6 respectively. From a general point of view, the simulations show that the three controllers have satisfactory and almost identical results with a small tracking error. The controllers having the CLFs with the quadratic form and the power factor 4 show the best robust performances while the one with the power factor 6 displays some destabilizing behavior when friction occurs. Future works must involve experimental simulations to confirm the actual results.

Conflict of Interest

The authors declare no conflict of interest.

Author Contributions

Honorine Angue Mintsa conducted the research, designed the controllers and wrote the paper; Gérémino Ella Eny designed the EHSS mathematical model and analyzed the data; Rolland Michel Assoumou Nzué and Nzamba Senouveau implemented the EHSS in the Matlab / Simulink environment and executed the numerical simulations. All authors had approved the final version.

References

[1] S. Zhao, *et al.*, "A generalized control model and its digital algorithm for aerospace electrohydraulic actuators," in *Proceedings*, vol. 64, no. 1, 2020, p. 31, MDPI.
[2] Amhmed M Al Aela, Jean-Pierre Kenne, and Honorine A Mintsa, "Adaptive neural network and nonlinear electrohydraulic active suspension control system," *Journal of Vibration and Control*, vol. 28, no. 3–4, pp. 243–259, 2022.
[3] S. Li, *et al.*, "Failure analysis for hydraulic system of heavy-duty machine tool with incomplete failure data," *Applied Sciences*, vol. 11, no. 3, p. 1249, 2021.
[4] S. S. Pachbhai and L. P Raut, "Design and development of hydraulic fixture for machining hydraulic lift housing," *Int. J. Mech. Eng. & Rob. Res.*, vol. 3, no. 3, p. 204, 2014.
[5] A. Chaijaruwanich and C. Thongthip, "Failure analysis of hydraulic rotary drill rods in a limestone mine," vol. 5, no. 4, 2016.
[6] C. M. Shern, R. Ghazali, C. S. Horng, H. I. Jaafar, and C. C. J. E. Soon, "Performance analysis of position tracking control with pid controller using an improved optimization technique," *Int. J. Mech. Eng. & Rob. Res.*, vol. 11, p. 12, 2019.
[7] A. D. Terenteva, "PID-control Systems on Single-bucket excavators during construction work in urban environments," *Int. J. Mech. Eng. & Rob. Res.*, vol. 10, no. 5, pp. 224–229, 2021.
[8] Z. Xiang, D. Ji, H. Zhang, H. Wu, and Y. J. I. S. Li, "A simple PID-based strategy for particle swarm optimization algorithm," *Information Sciences*, vol. 502, pp. 558–574, 2019.
[9] H. E. Merritt, *Hydraulic Control Systems*, John Wiley & Sons Inc, 1967.
[10] M. Krstic, P. V. Kokotovic, and I. Kanellakopoulos, *Nonlinear and Adaptive Control Design*. John Wiley & Sons, Inc., 1995.
[11] C. Kaddissi, J. P. Kenne, and M. Saad, "Identification and real-time control of an electrohydraulic servo system based on nonlinear backstepping," *IEEE/ASME Transactions on Mechatronics*, vol. 12, no. 1, pp. 12–22, 2007.
[12] M. F. Ghani *et al.*, "Improved third order PID sliding mode controller for electrohydraulic actuator tracking control," *Journal of Robotics and Control*, vol. 3, no. 2, pp. 219–226, 2022.
[13] H. A. Mintsa, G. E. Eny, N. Senouveau, J. P. Kenné and R. M. Assoumou Nzué, "An alternative nonlinear Lyapunov redesign velocity controller for an electrohydraulic drive," *Journal of Robotics and Control*, vol. 4, no. 2, pp. 192–201, 2023.
[14] J. Mawhin and A. M. Liapunov, *The General Problem of the Stability of Motion (1892)*, 2005, pp. 664–676.
[15] D. Koditschek, "The application of total energy as a Lyapunov function for mechanical control systems," vol. 97, p. 131, 1989.
[16] N. T. Binh, N. A. Tung, D. P. Nam, and N. H. Quang, "An adaptive backstepping trajectory tracking control of a tractor trailer wheeled mobile robot," *International Journal of Control, Automation and Systems*, vol. 17, no. 2, pp. 465–473, 2019.
[17] H. A. Mintsa, R. Venugopal, Jean-Pierre Kenne, C. Belleau, "Feedback linearization-based position control of an electrohydraulic servo system with supply pressure uncertainty," *IEEE Transactions on Control Systems Technology*, vol. 20, no. 4, pp. 1092–1099, 2011.
[18] M. F. Ghani, *et al.*, "Fractional order integral sliding mode tracking control of a third-order double-acting electrohydraulic actuator model," *Int. J. Mech. Eng. & Rob. Res.*, vol. 11, no. 9, 2022.

[19] Z. Artstein, "Stabilization with relaxed controls," *Nonlinear Analysis: Theory, Methods &* Applications, vol. 7, no. 11, pp. 1163–1173, 1983.
[20] E. D. Sontag, "A 'universal' construction of Artstein's theorem on nonlinear stabilization," *Systems & Control Letters*, vol. 13, no. 2, pp. 117–123, 1989.
[21] J. J. E. Slotine and W. Li, *Applied Nonlinear Control*, Prentice hall Englewood Cliffs, NJ, no. 1, 1991.
[22] P. T. Phuc, T. P. Tho, N. D. X. Hai, and N. T. Thinh, "Design of adaptive fuzzy sliding mode controller for mobile robot," *International Journal of Mechanical Engineering and Robotics Research*, vol. 10, no. 2, pp. 54–59, 2021.
[23] R. Almeida, R. P. Agarwal, S. Hristova, and D. O'Regan, "Quadratic Lyapunov functions for stability of the generalized proportional fractional differential equations with applications to neural networks," *Axioms*, vol. 10, no. 4, p. 322, 2021.
[24] S. Asadi, "Robust sliding mode observer design for simultaneous fault reconstruction in perturbed Takagi-Sugeno fuzzy systems using non-quadratic stability analysis," *Journal of Vibration and Control*, vol. 26, no. 11-12, pp. 1092–1105, 2020.
[25] F. Shokouhi and A. H. Davaie Markazi, "A new continuous approximation of sign function for sliding mode control," in *Proc. International Conference on Robotics and Mechatronics (ICRoM 2018)*. Tehran. Iran, 2018.
[26] H. Angue-Mintsa, R. Venugopal, Jean-Pierre Kenné, C. Belleau, "Adaptive position control of an electrohydraulic servo system with load disturbance rejection and friction compensation," *Journal of Dynamic System, Measurement, and Control*, vol. 133, no. 6, 2011.
[27] M. A. Gomez, C. D. Cruz-Ancona, L Fridman, "Super twisting based Lyapunov redesign for uncertain linear delay systems," *IEEE Transactions on Automatic Control*, vol. 68, no. 2, pp. 1107–1113, 2022.
[28] E. Jalalabadi, S. Z. Paylakhi, A. Rahimi-kian, and B. Moshiri, "Integral backstepping Lyapunov redesign control of uncertain nonlinear systems," *IET Control Theory & Applications*, vol. 16, no. 3, pp. 330–339, 2022.
[29] G. Guo and R. Zhang, "Lyapunov redesign-based optimal consensus control for multi-agent systems with uncertain dynamics," *IEEE Transactions on Circuits and Systems II: Express Briefs*, vol. 69, no. 6, pp. 2902–2906, 2022.